

# Thermal evolution of hybrid stars within the framework of a non-local NJL model

S. M. de Carvalho<sup>1,2</sup>, R. Negreiros<sup>2</sup>, M. Orsaria<sup>3,4</sup>, G. A. Contrera<sup>3,4,5</sup>, F. Weber<sup>6,7</sup> and W. Spinella<sup>6,8</sup>

<sup>1</sup>*ICRANet-Rio, Centro Brasileiro de Pesquisas Físicas,*

*Rua Dr. Xavier Sigaud 150, Rio de Janeiro, RJ, 22290-180, Brazil*

<sup>2</sup>*Instituto de Física, Universidade Federal Fluminense, UFF, Niterói, 24210-346, RJ, Brazil*

<sup>3</sup>*CONICET, Rivadavia 1917, 1033 Buenos Aires, Argentina*

<sup>4</sup>*Grupo de Gravitación, Astrofísica y Cosmología,*

*Facultad de Ciencias Astronómicas y Geofísicas, Universidad Nacional de La Plata,*

*Paseo del Bosque S/N (1900), La Plata, Argentina*

<sup>5</sup>*IFLP, CONICET - Dpto. de Física, UNLP, La Plata, Argentina*

<sup>6</sup>*Department of Physics, San Diego State University,*

*5500 Campanile Drive, San Diego, California 92182*

<sup>7</sup>*Center for Astrophysics and Space Sciences,*

*University of California,*

*San Diego, La Jolla, CA 92093, USA and*

<sup>8</sup>*Computational Science Research Center, San Diego State University,*

*5500 Campanile Drive, San Diego, California 92182*

(Dated: January 13, 2016)

We study the thermal evolution of neutron stars containing deconfined quark matter in their core. Such objects are generally referred to as quark-hybrid stars. The confined hadronic matter in their core is described in the framework of non-linear relativistic nuclear field theory. For the quark phase we use a non-local extension of the SU(3) Nambu Jona-Lasinio model with vector interactions. The Gibbs condition is used to model phase equilibrium between confined hadronic matter and deconfined quark matter. Our study indicates that high-mass neutron stars may contain between 35 and 40% deconfined quark-hybrid matter in their cores. Neutron stars with canonical masses of around  $1.4 M_{\odot}$  would not contain deconfined quark matter. The central proton fractions of the stars are found to be high, enabling them to cool rapidly. Very good agreement with the temperature evolution established for the neutron star in Cassiopeia A (Cas A) is obtained for one of our models (based on the popular NL3 nuclear parametrization), if the protons in the core of our stellar models are strongly paired, the repulsion among the quarks is mildly repulsive, and the mass of Cas A has a canonical value of  $1.4 M_{\odot}$ .

## I. INTRODUCTION

Exploring the properties of compressed baryonic matter, or, more generally, strongly interacting matter at high densities and/or temperatures, has become a forefront area of modern physics. Experimentally, the properties of such matter are being probed with the Relativistic Heavy Ion Collider RHIC at Brookhaven and the Large Hadron Collider LHC at Cern. Great advances in our understanding of such matter are also expected from the next generation of heavy-ion collision experiments at FAIR (Facility for Antiproton and Ion Research at GSI) and NICA (Nuclotron-based Ion Collider fAcility at JINR) [1, 2] as well as from the study of neutron stars (for an overview, see [1, 3–15] and references therein).

Neutron stars (NSs) contain nuclear matter compressed to densities which are several times higher than the densities of atomic nuclei. At such extreme conditions, the fundamental building blocks of matter may no longer be just neutrons and protons immersed in a gas of relativistic electron and muons, but other nuclear degrees of freedom such as hyperons, delta particles and, most intriguingly, deconfined up, down and strange quarks may begin to play a role. Neutron stars containing deconfined quark matter in their central core are referred to as quark-hybrid stars (hybrid stars, for short).

The most massive neutron stars observed to date are  $J1614 - 2230$  ( $1.97 \pm 0.04 M_{\odot}$ ) [16] and  $J0348 + 0432$  ( $2.01 \pm 0.04 M_{\odot}$ ) [17]. In several recent papers [18–24], it has been shown that they may contain significant fractions of quark-hybrid matter in their centers, despite the relatively stiff nuclear equation of state (EoS) that is required to achieve such high masses. The radii of these neutron stars would be between 13 and 14 km, depending on the nuclear EoS [18, 19], increasing to respectively 13.5 and 14.5 km for lighter neutron stars with canonical masses of around  $1.4 M_{\odot}$ . Such radius values lie between the radius determinations based on X-ray burst oscillations of neutron stars in low-mass X-ray binaries [25–28] and the estimates of the radius of the isolated neutron star RX J1856-3754 [29], emitting purely thermal radiation in the X-ray and in the optical bands.

If the dense interior of a neutron star contains deconfined quark matter, it will most likely be three-flavor quark matter, since such matter has lower energy than two-flavor quark matter [30, 31]. Furthermore, just as for the hyperon content of neutron stars, strangeness is not conserved on macroscopic time scales which allows neutron stars to convert confined hadronic matter to three-flavor quark matter until equilibrium brings this process to a halt. We considered the transition from hadronic to quark matter to be first order. There are two distinct

ways to construct a first order phase transition in neutron stars. The first option is a Gibbs construction, where the electronic and baryonic chemical potentials as well as the pressure are continuous during the phase transition; the second option is a Maxwell construction, where only the baryonic chemical potential and pressure are continuous and the electronic chemical potential is characterized by a discontinuity at the phase boundary. The surface tension at the interface between the quark-hadron phase is what determines whether a Gibbs or Maxwell phase transition may be taking place. Several authors [34–39] have attempted to estimate the value of the surface tension, with mixed results. For what follows, we will assume that the surface tension is less than  $40 \text{ MeV fm}^{-2}$ , such that the Gibbs condition is favored and a mixed phase of quark matter and nuclear matter exists above a certain density [40].

In the mixed phase, the presence of quarks allows the hadronic component to become more isospin symmetric, which is accomplished by the transference of electric charge to the quark phase. Thus, the symmetry energy can be lowered at only a small cost in rearranging the quark Fermi surfaces. The implication of this charge rearrangement is that the mixed phase region of a neutron star will have positively charged hadronic matter and negatively charged quark matter [3, 31, 41]. This should have important implications for the electric and thermal properties of NSs. Studies of the transport properties of quark-hybrid neutron star matter have been reported in [42, 43].

As already mentioned above, this study is carried out for neutron stars containing deconfined quark matter in their centers (so-called quark-hybrid stars). To describe the quark matter phase, we use a non-local extension of the SU(3) Nambu Jona-Lasinio (NJL) model [44–47] with vector interactions. For the hadronic phase we consider a non-linear relativistic mean-field model [48–52] solved for two different parametrizations, GM1 [53] and NL3 [54]. The transition from the confined hadronic phase to the deconfined quark phase is treated as a Gibbs transition, imposing global electric charge neutrality and baryon number conservation on the field equations. We find that the non-local NJL model predicts the existence of extended regions of mixed quark-hadron (quark-hybrid) matter in neutron stars with masses up to  $2.4 M_\odot$ .

The paper is organized as follows. In Sect. II, we describe the non-local extension of the SU(3) NJL model at zero temperature. In Sect. III, the non-linear relativistic mean-field model, which is used for the description of confined hadronic matter, is briefly discussed. In Sect. IV, the construction of the quark-hadron mixed phase is discussed for neutron star matter characterized by global charge neutrality. Our results for the global structure and composition of quark-hybrid stars are discussed

in Sects. V. A discussion of their thermal evolution is presented in VI. Finally, a summary of our results and important conclusions are provided in Sect. VII.

## II. QUARK MATTER PHASE

In this section we briefly describe the non-local extension of the SU(3) Nambu Jona-Lasinio (n3NJL) model. The Euclidean effective action for the quark sector, including the vector coupling interaction, is given by

$$S_E = \int d^4x \left\{ \bar{\psi}(x) [-i\partial + \hat{m}] \psi(x) - \frac{G_S}{2} [j_a^S(x) j_a^S(x) + j_a^P(x) j_a^P(x)] - \frac{G_P}{4} T_{abc} [j_a^S(x) j_b^S(x) j_c^S(x) - 3 j_a^S(x) j_b^P(x) j_c^P(x)] - \frac{G_V}{2} [j_{Va}^\mu(x) j_{Va}^\mu(x)] \right\}, \quad (1)$$

where  $\psi$  stands for the light quark fields,  $\hat{m}$  denotes the current quark mass matrix, and  $G_S$ ,  $G_P$  and  $G_V$  are the scalar, pseudo-scalar, and vector coupling constant of the theory, respectively. For simplicity, we consider the isospin symmetric limit in which  $m_u = m_d = \bar{m}$ . The operator  $\partial = \gamma_\mu \partial_\mu$  in Euclidean space is defined as  $\vec{\gamma} \cdot \vec{\nabla} + \gamma_4 \frac{\partial}{\partial \tau}$ , with  $\gamma_4 = i\gamma_0$ . The scalar ( $S$ ), pseudo-scalar ( $P$ ), and vector ( $V$ ) current densities  $j_a^S(x)$ ,  $j_a^P(x)$ , and  $j_{Va}^\mu(x)$ , respectively, are given by

$$j_a^S(x) = \int d^4z \tilde{g}(z) \bar{\psi} \left( x + \frac{z}{2} \right) \lambda_a \psi \left( x - \frac{z}{2} \right), \\ j_a^P(x) = \int d^4z \tilde{g}(z) \bar{\psi} \left( x + \frac{z}{2} \right) i \gamma_5 \lambda_a \psi \left( x - \frac{z}{2} \right), \\ j_{Va}^\mu(x) = \int d^4z \tilde{g}(z) \bar{\psi} \left( x + \frac{z}{2} \right) \gamma^\mu \lambda_a \psi \left( x - \frac{z}{2} \right), \quad (2)$$

where  $\tilde{g}(z)$  is a form factor responsible for the non-local character of the interaction,  $\lambda_a$  with  $a = 1, \dots, 8$  denotes the generators of SU(3), and  $\lambda_0 = \sqrt{2/3} \mathbb{1}_{3 \times 3}$ . Finally, the constants  $T_{abc}$  in the t'Hooft term accounting for flavor-mixing are defined by

$$T_{abc} = \frac{1}{3!} \epsilon_{ijk} \epsilon_{mnl} (\lambda_a)_{im} (\lambda_b)_{jn} (\lambda_c)_{kl}. \quad (3)$$

After the standard bosonization of Eq. (1), the integrals over the quark fields can be performed in the framework of the Euclidean four-momentum formalism. Thus, the grand canonical thermodynamical potential of the model within the mean field approximation at zero temperature is given by

$$\Omega^{NL}(M_f, \mu_f) = -\frac{N_c}{\pi^3} \sum_{f=u,d,s} \int_0^\infty dp_0 \int_0^\infty dp \ln \left\{ [\hat{\omega}_f^2 + M_f^2(\omega_f^2)] \frac{1}{\omega_f^2 + m_f^2} \right\} \quad (4)$$

$$-\frac{N_c}{\pi^2} \sum_{f=u,d,s} \int_0^{\sqrt{\mu_f^2 - m_f^2}} dp p^2 [(\mu_f - E_f)\Theta(\mu_f - m_f)] - \frac{1}{2} \left[ \sum_{f=u,d,s} (\bar{\sigma}_f \bar{S}_f + \frac{G_S}{2} \bar{S}_f^2) + \frac{G_P}{2} \bar{S}_u \bar{S}_d \bar{S}_s \right] - \sum_{f=u,d,s} \frac{\varpi_f^2}{4G_V},$$

where  $N_c = 3$ ,  $E_f = \sqrt{p^2 + m_f^2}$ ,  $\omega_f^2 = (p_0 + i\mu_f)^2 + p^2$ , and  $\bar{\sigma}_f$  denotes the mean-field values of the quark flavor ( $f = u, d, s$ ) fields. The vector coupling constant  $G_V$  is treated as a free parameter and expressed as a fraction of the strong coupling constant  $G_S$ .

The constituent quark masses  $M_f$  are treated as momentum-dependent quantities. They are given by

$$M_f(\omega_f^2) = m_f + \bar{\sigma}_f g(\omega_f^2), \quad (5)$$

where  $g(\omega_f^2)$  is the Fourier transform of the form factor  $\tilde{g}(z)$ . The vector mean fields  $\varpi_f$  are associated with the vector current densities  $j_{V_a}^\mu(x)$ , where a different vector field for each quark flavor  $f$  has been considered.

We followed the method described in [55] to include the vector interactions. The inclusion of vector interactions shifts the quark chemical potential as follows,

$$\hat{\mu}_f = \mu_f - g(\omega_f^2)\varpi_f, \quad (6)$$

$$\hat{\omega}_f^2 = (p_0 + i\hat{\mu}_f)^2 + p^2. \quad (7)$$

Note that the shift in the quark chemical potential does not affect the Gaussian non-local form factor,

$$g(\omega_f^2) = \exp(-\omega_f^2/\Lambda^2), \quad (8)$$

avoiding a recursive problem as discussed in [55–57]. In Eq. (8),  $\Lambda$  plays the role of an ultraviolet cut-off momentum scale and is taken as a parameter which, together with the quark current masses and coupling constants  $G_S$  and  $G_P$  in Eq. (1), can be chosen so as to reproduce the phenomenological values of pion decay constant  $f_\pi$ , and the meson masses  $m_\pi$ ,  $m_\eta$ ,  $m_{\eta'}$ , as described in [46, 47]. In this work we use the same parameters as in [18, 19].

For the stationary phase approximation [45], the mean-field values of the auxiliary fields  $\bar{S}_f$  in Eq. (4) are given by

$$\bar{S}_f = -4N_c \int_0^\infty \frac{dp_0}{2\pi} \int \frac{d^3p}{(2\pi)^3} g(\omega_f^2) \frac{M_f(\omega_f^2)}{\hat{\omega}^2 + M_f^2(\omega_f^2)}. \quad (9)$$

Due to the charge neutrality constraint, we consider three scalar fields,  $\bar{\sigma}_u$ ,  $\bar{\sigma}_d$  and  $\bar{\sigma}_s$ , which can be obtained by solving the coupled system of “gap” equations [45] given

by

$$\begin{aligned} \bar{\sigma}_u + G_S \bar{S}_u + \frac{G_P}{2} \bar{S}_d \bar{S}_s &= 0, \\ \bar{\sigma}_d + G_S \bar{S}_d + \frac{G_P}{2} \bar{S}_u \bar{S}_s &= 0, \\ \bar{\sigma}_s + G_S \bar{S}_s + \frac{G_P}{2} \bar{S}_u \bar{S}_d &= 0. \end{aligned} \quad (10)$$

The vector mean fields  $\varpi_f$  are obtained by minimizing Eq. (4), i.e.  $\frac{\partial \Omega^{NL}}{\partial \varpi_f} = 0$ .

For quark matter in chemical equilibrium at finite density, the basic particle processes involved are given by the strong process  $u + d \leftrightarrow u + s$  as well as the weak processes  $d(s) \rightarrow u + e^-$  and  $u + e^- \rightarrow d(s)$ . We are assuming that neutrinos, once created by weak reactions, leave the system, which is equivalent to supposing that the neutrino chemical potential is equal to zero. Therefore, the chemical potential for each quark flavor  $f$  is given by

$$\mu_f = \mu_b - Q\mu_e, \quad (11)$$

where  $Q = \text{diag}(2/3, -1/3, -1/3)$  in flavor space and  $\mu_b = 1/3 \sum_f \mu_f$  is the baryonic chemical potential.

The contribution of free degenerate leptons to the quark phase is given by

$$\Omega_{\lambda=e^-, \mu^-}(\mu_e) = -\frac{1}{\pi^2} \int_0^{p_{F\lambda}} p^2 \left( \sqrt{p^2 + m_\lambda^2} - \mu_e \right) dp. \quad (12)$$

Muons appear in the system if the electron chemical potential  $\mu_e = \mu_\mu$  is greater than the muon rest mass,  $m_\mu = 105.7$  MeV. For electrons we have  $m_e = 0.5$  MeV. Thus, the total thermodynamic potential of the quark phase is given by Eq. (4) supplemented with the leptonic contribution of Eq. (12).

### III. CONFINED HADRONIC MATTER

The hadronic phase is described in the framework of the non-linear relativistic nuclear field theory [48–52], where baryons (neutrons, protons, hyperons and delta states) interact via the exchange of scalar, vector and isovector mesons ( $\sigma$ ,  $\omega$ ,  $\rho$ , respectively). The parametrizations used in our study are GM1 [53] and NL3 [54]. The lagrangian of this model is given by

$$\mathcal{L} = \mathcal{L}_H + \mathcal{L}_\ell, \quad (13)$$

with the leptonic lagrangian given by

$$\mathcal{L}_\ell = \sum_{\lambda=e^-, \mu^-} \bar{\psi}_\lambda (i\gamma_\mu \partial^\mu - m_\lambda) \psi_\lambda. \quad (14)$$

---


$$\begin{aligned} \mathcal{L}_H = & \sum_{B=n,p,\Lambda,\Sigma,\Xi} \bar{\psi}_B [\gamma_\mu (i\partial^\mu - g_\omega \omega^\mu - g_\rho \vec{\rho}_\mu) - (m_N - g_\sigma \sigma)] \psi_B + \frac{1}{2} (\partial_\mu \sigma \partial^\mu \sigma - m_\sigma^2 \sigma^2) - \frac{1}{3} b_\sigma m_N (g_\sigma \sigma)^3 - \frac{1}{4} c_\sigma (g_\sigma \sigma)^4 \\ & - \frac{1}{4} \omega_{\mu\nu} \omega^{\mu\nu} + \frac{1}{2} m_\omega^2 \omega_\mu \omega^\mu + \frac{1}{2} m_\rho^2 \vec{\rho}_\mu \cdot \vec{\rho}^\mu - \frac{1}{4} \vec{\rho}_{\mu\nu} \vec{\rho}^{\mu\nu}. \end{aligned} \quad (15)$$


---

The quantity  $B$  sums over all baryonic states which become populated in neutron star matter at a given density [3, 4]. Intriguingly, we have found that, aside from hyperons, the  $\Delta^-$  state becomes populated in neutron star matter at densities that could be reached in the cores of stable neutron stars [19]. Simpler treatments of the quark-hadron phase transition, based on the MIT bag model [31, 41] do not predict the occurrence of the  $\Delta^-$  state in stable neutron stars.

For the models of this paper,  $\Delta$  states become populated when the vector repulsion among quarks reaches values of  $G_V \gtrsim 0.05 G_S$ , leading to a substantial stiffening of the EoS. This stiffening more than offsets the softening of the EoS caused the generation of the  $\Delta$  states, resulting in an EoS which is readily capable to accommodate even very heavy ( $2 M_\odot$ ) neutron stars. Without this additional stiffening, it would be difficult to account for  $2 M_\odot$  neutron stars with equations of state that are characterized by an early appearance of  $\Delta$ 's, at densities between around 2 to 3 times nuclear saturation density [58].

#### IV. QUARK-HADRON MIXED PHASE

To determine the mixed phase region of quarks and hadrons we start from the Gibbs condition for pressure equilibrium between confined hadronic ( $P^H$ ) matter and deconfined quark ( $P^q$ ) matter. The Gibbs condition is given by

$$P^H(\mu_b^H, \mu_e^H, \{\phi\}) = P^q(\mu_b^q, \mu_e^q, \{\psi\}), \quad (16)$$

with  $\mu_b^H = \mu_b^q$  for the baryon chemical potentials and  $\mu_e^H = \mu_e^q$  for the electron chemical potentials in the hadronic ( $H$ ) and quark ( $q$ ) phase. The quantities  $\{\phi\}$  and  $\{\psi\}$  stand collectively for the field variables and Fermi momenta that characterize the solutions to the equations of confined hadronic matter and deconfined quark matter, respectively. By definition, the quark chemical potential is given by  $\mu_b^q = \mu_n/3$ , where  $\mu_n$  is the chemical potential of the neutrons. In the mixed phase, the baryon number density,  $n_b$ , and the energy density,  $\varepsilon$ , are given by

$$n_b = (1 - \chi) n_b^H + \chi n_b^q, \quad (17)$$

The hadronic lagrangian has the form

and

$$\varepsilon = (1 - \chi) \varepsilon^H + \chi \varepsilon^q, \quad (18)$$

where  $n_b^H$  ( $\varepsilon^H$ ) and  $n_b^q$  ( $\varepsilon^q$ ) denote the baryon number (energy) densities of the hadronic and the quark phase, respectively. The quantity  $\chi \equiv V_q/V$  denotes the volume proportion of quark matter,  $V_q$ , in the unknown volume  $V$ . Therefore, by definition  $\chi$  varies from 0 to 1 depending on how much confined hadronic matter has been converted to quark matter at a given density. The condition of global electric charge neutrality is given by the equation

$$(1 - \chi) \sum_{i=B,l} q_i^H n_i^H + \chi \sum_{i=q,l} q_i^q n_i^q = 0, \quad (19)$$

where  $q_i$  is the electric charge of particle species  $i$ , expressed in units of the electron charge. Because of the global conservation of electric charge and baryonic number, the pressure in the mixed phase increases monotonically with increasing energy density, as shown in Fig. 1. In this work we have chosen global rather than local electric charge neutrality, since the latter is not fully consistent with the Einstein-Maxwell equations and the micro-physical condition of chemical equilibrium and relativistic quantum statistics, as shown in [59]. In contrast to local electric charge neutrality, the global neutrality condition puts a net positive electric charge on hadronic matter, rendering it more isospin symmetric, and a net negative electric charge on quark matter, allowing neutron star matter to settle down in a lower energy state that otherwise possible [31, 41].

#### V. STRUCTURE OF NEUTRON STARS

We now turn to the discussion of the structure of neutron stars, which are computed for the microscopic models of quark-hybrid matter discussed in Sect. II and III. We shall explore three values for the vector coupling constant  $G_V/G_S$ , i.e. 0, 0.05, and 0.09. The mass-radius relationships of these stars are shown in Fig. 2. One sees that increasing values of  $G_V$  lead to higher maximum masses for both equations of state (GM1 and NL3)

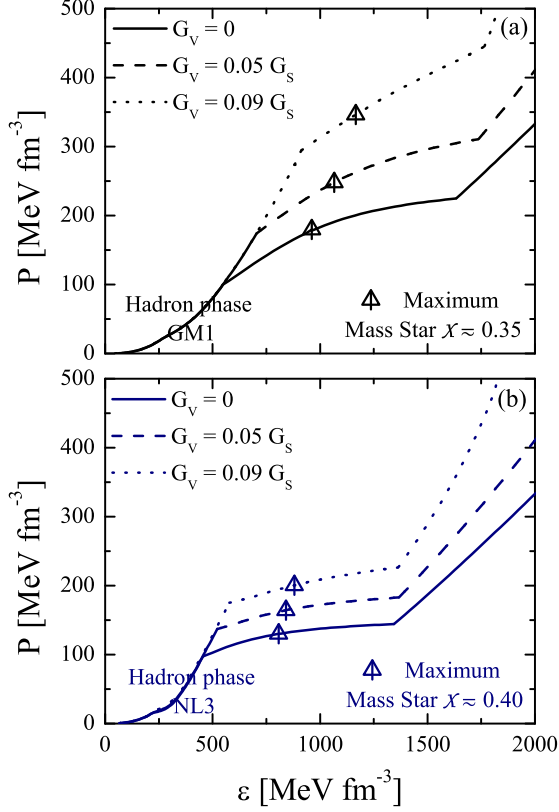


Figure 1: (Color online) Pressure,  $P$ , as a function of the energy density,  $\epsilon$ , for the different nuclear parametrizations (GM1, NL3) and vector coupling constant  $G_V/G_S$  (0, 0.05, 0.09) considered in this paper. Panel (a) shows the hybrid EoSs computed for GM1, panel (b) shows the hybrid EoSs computed for NL3. The triangles in both panels indicate the central densities of the maximum-mass neutron stars (see Fig. 2) associated with each EoS. The quantity  $\chi$  denotes the fraction of quark matter inside of the most massive neutron star for each EoS.

studied in this work. This is expected, since the stiffness of the equation of state increases with  $G_V$ . We also note that all neutron stars computed for NL3 have larger radii than those obtained for the GM1 parametrization. This is so because the NL3 equation of state is stiffer than the GM1 equation of state, leading to quark deconfinement at densities that are lower than for the GM1 parametrization, as can be seen in Fig. (1). This figure also shows that the neutron stars close to the mass peaks possess extended mixed phase regions with approximately 40% quark matter for NL3 and 35% quark matter for GM1. In addition, we find that calculations carried out for GM1 and a vanishingly small value of  $G_V$  lead to neutron star masses of around  $1.8 M_\odot$ , which is well below the masses observed for neutron stars J1614-2230 ( $1.97 \pm 0.04 M_\odot$ ) [16] and J0348+0432 ( $2.01 \pm 0.04 M_\odot$ ) [17]. Therefore, this combination of model parameters for the equation of state can be ruled out. The calculations have been carried out using a combination of the

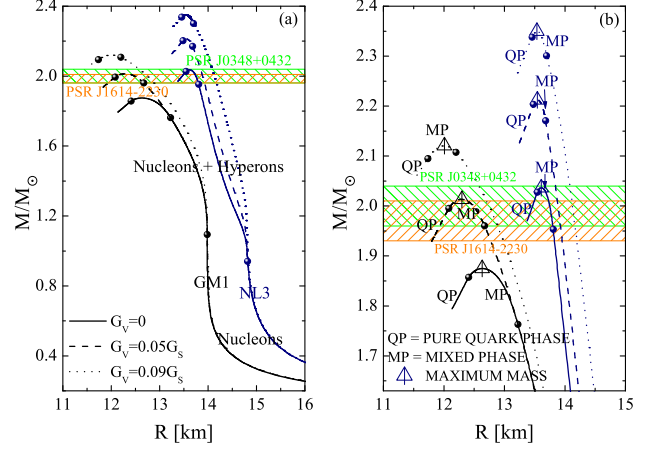


Figure 2: (Color online) (a) Mass-radius relationships of neutron stars made of quark-hybrid matter. (b) Enlargement of the maximum mass region of (a). The labels GM1 and NL3 label the hadronic model for the EoS,  $G_V$  indicates the strength of the vector coupling constant among quarks.

Baym-Pethick Sutherland [32] and Baym-Bethe-Pethick [33] EoS at sub-saturation densities.

## VI. THERMAL EVOLUTION

We now turn our attention to the thermal evolution of neutron stars whose structure and interior composition are given by the microscopic models described in the previous sections.

Here we briefly describe the thermal evolution equations that govern the cooling of neutron stars. The thermal balance and transport equations for a general relativistic, spherically symmetric object is given by

$$\frac{\partial(Le^\nu)}{\partial r} = -\frac{4\pi r^2}{\sqrt{1-2m/r}} \left[ \epsilon_\nu e^\nu + c_\nu \frac{\partial(Te^{\nu/2})}{\partial t} \right], \quad (20)$$

$$\frac{Le^\nu}{4\pi r^2 \kappa} = \sqrt{1-2m/r} \frac{\partial(Te^{\nu/2})}{\partial r}, \quad (21)$$

where  $r$ ,  $m(r)$ ,  $\rho(r)$ , and  $\nu(r)$  represent the radial distance, mass, energy density, and gravitational potential, respectively. Furthermore, the thermal variables are given by the interior temperature  $T(r, t)$ , the luminosity  $L(r, t)$ , neutrino emissivity  $\epsilon_\nu(r, T)$ , thermal conductivity  $\kappa(r, T)$ , and the specific heat per unit volume  $c_\nu(r, T)$ .

The solution of Eqs. (20)–(21) is obtained with the help of two boundary conditions, one at the core, where the luminosity vanishes,  $L(r=0) = 0$ , since the heat flux there is zero. The second boundary condition has to do with the surface luminosity, which is defined by the relationship between the mantle temperature and the surface temperature [60–62]. Furthermore we consider all neutrino emission processes relevant to the thermal evolution of compact stars, including the Pair Breaking and Formation process (PBF) responsible for a splash



of neutrinos on the onset of pair formation. We now describe pairing effects and its corresponding effects on the thermal evolution on the quark-hybrid stars discussed in this paper.

### A. Pairing Models

In addition to the microscopic model described in the previous sections, we now devote some time to the discussion of pairing of nucleons, which will be used in our cooling simulations below. Pairing among nucleons has received enormous interest recently due to the unusual thermal data observed for the neutron star in Cassiopeia A (Cas A) (see e.g. [63–65] for a recent study of the effects of pairing in the thermal evolution of compact stars).

A full-blown microscopic description of pairing among neutrons and protons in beta stable matter at high densities is a challenging task, and so far there are still many uncertainties, particularly with respect to proton-pairing at high-densities [66]. In this work we use a phenomenological description, as described in [67]. We assume that neutrons form singlet  $^1S_0$  pairs in the crust and triplet  $^3P_2$  pairs in the core.

As for the protons, there is still much discussion as to how high densities protons may form pairs in the cores of neutron stars. As discussed in [68], the presence of the direct Urca process in the core of neutron stars depends strongly on the symmetry energy and on its possible dependence on a so-called “quartic term” (a term that is of fourth order in the deviation from symmetric matter). As pointed out in [68], it is very difficult to interpret neutron star cooling without more information regarding the symmetry energy and its “quartic term” dependence at high densities. For that reason we have chosen to study three different models for proton pairing, which are re-

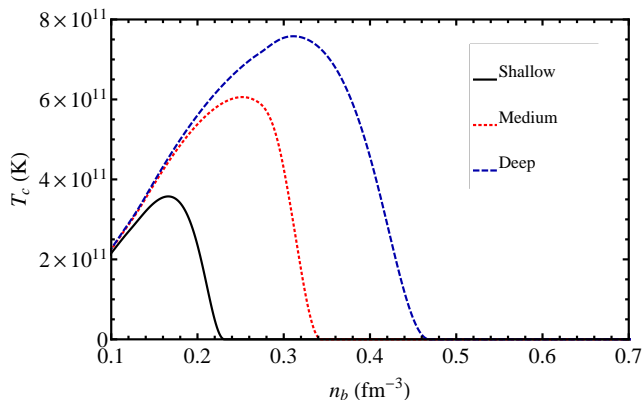


Figure 3: (Color online) Critical temperature,  $T_C$ , for the onset of proton ( $^1S_0$ ) singlet pairing in neutron star matter as a function of baryon number density,  $n_b$ .

ferred to as shallow, medium, and deep. As the labeling indicates, these models correspond to proton pairing that ends at low, medium and high densities, respectively. In

Table I: Properties of the neutron stars whose thermal evolutions are investigated for the nuclear parametrizations (GM1 and NL3) of this paper.  $G_V$  is the vector coupling constant among quarks,  $M$  and  $R$  denote the neutron stars’ gravitational masses and radii, respectively.

Parametrization	$G_V/G_S$	$M [M_\odot]$	$R [\text{km}]$	$\rho_c [\text{MeV}/\text{fm}^3]$
GM1	0	1.4	13.84	375.27
		1.87	12.63	961.10
GM1	0.05	1.4	13.85	375.27
		2.0	12.48	819.58
GM1	0.09	1.4	13.91	355.08
		2.0	12.74	443.28
NL3	0	1.4	14.32	343.30
		2.0	13.75	541.10
NL3	0.05	1.4	14.47	333.76
		2.2	13.62	675.07
NL3	0.09	1.4	14.68	311.33
		2.0	14.12	693.88

Fig. 3 we show the critical temperature for the three models used for proton  $^1S_0$  singlet pairing in the cores of the stars studied in this paper.

### B. Neutron Star Cooling Curves

We now show the thermal evolution obtained by numerically integrating the energy balance and transport equations (20)–(21). We have chosen to perform simulations on two different neutron stars; the first has a gravitational mass of  $1.4 M_\odot$ , and the second has a mass that is closer to the maximum-mass value of each stellar sequence. The thermal evolution of neutron stars with masses between these two limiting cases will then lie within the bounds of these two cooling curves. In Table I we show the properties of the neutron stars whose thermal evolution is being studied.

We show in Fig. 4 the surface temperature  $T_s$  as a function of time  $t$  (in years) for the GM1 parametrization. The results for the NL3 parametrization are shown in Fig. 5. Figure 4 shows that the shallow and medium proton pairing cases obtained for the GM1 parametrization exhibit very little difference. For both cases pairing is not strong enough to completely suppress all fast neutrino processes so that these stars exhibit fast cooling. Stars with a lower mass show slightly slower cooling due to their smaller core densities (and thus smaller proton fractions). The situation is different for the deep pairing model where only for the lighter stars ( $G_V = 0$  and  $G_V = 0.05 G_S$ ) the neutrino process is completely suppressed. Furthermore, for the deep pairing model, all stars obtained for  $G_V = 0.09 G_S$  have their fast neutrino processes suppressed.

As for the NL3 parametrization, Fig. 5 shows that the

shallow and medium cases have similar behavior in that there is no complete suppression of the fast neutrino processes. The deep case, however, exhibits a behavior that is somewhat opposite to what we found for the GM1 parametrization. One sees that the fast neutrino processes are totally suppressed in both light and heavy neutron stars when  $G_V = 0$  and  $G_V = 0.05 G_S$ . In contrast to this, when  $G_V = 0.09 G_S$  we see that the fast neutrino processes are only suppressed in lighter neutron stars.

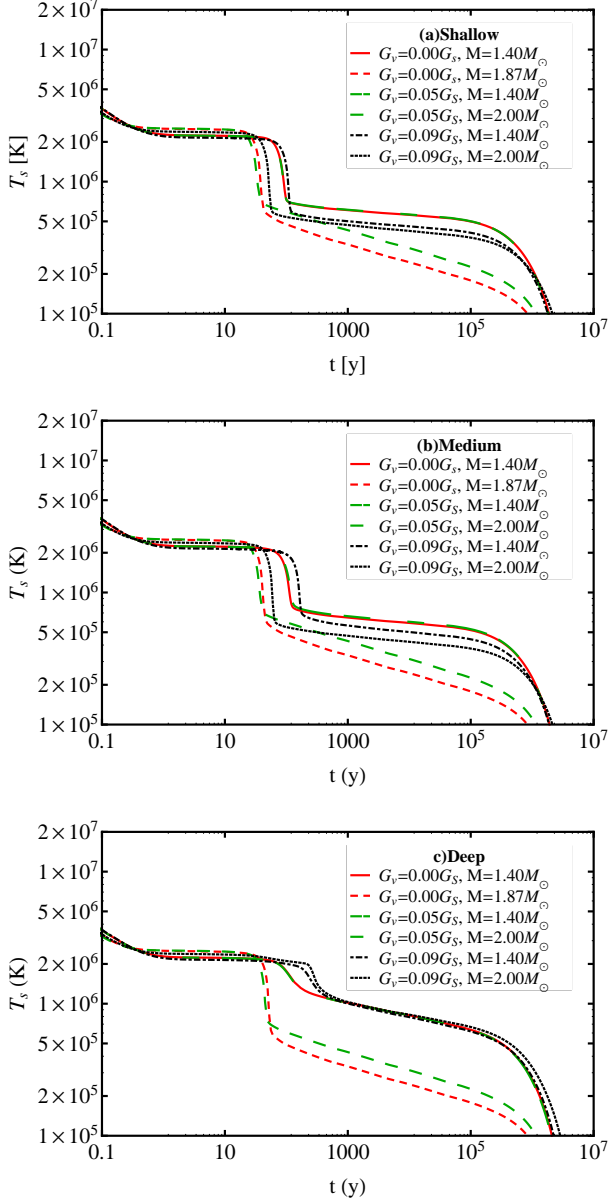


Figure 4: (Color online) Thermal evolution of neutron stars for the different proton pairing scenarios (shallow, medium, and deep) considered in this paper. The calculations are carried out for the GM1 parametrization and vector coupling constants ranging from zero to  $0.09 G_S$ .

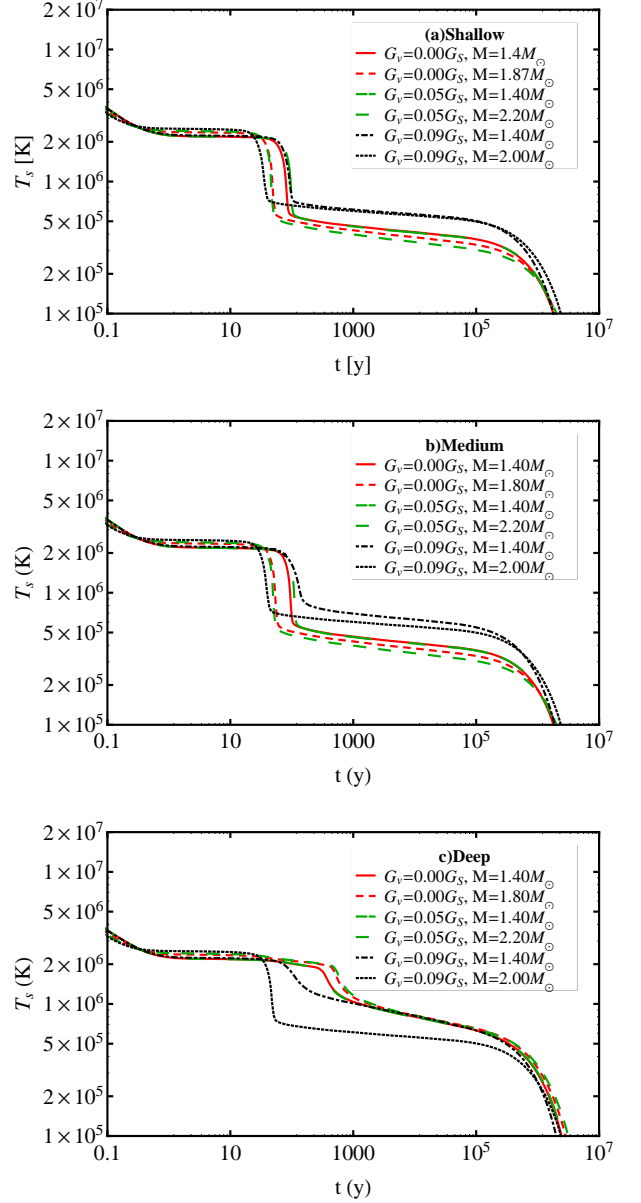


Figure 5: (Color online) Same as Fig. 4, but for the NL3 parametrization.

### C. Comparison with Observed Data

We complete our study of the thermal evolution by comparing our results with the thermal behavior observed for compact stars, and, in particular, that of the neutron stars in Cassiopeia A (Cas A). This object is the youngest known neutron star from which the thermal emission has been observed continuously for a decade. Heinke & Ho found that the surface temperature of Cas A has dropped by 4% between 2000 and 2009, from  $2.12$  to  $2.04 \times 10^6$  K [69]. The rapid cooling has been attributed to the onset of neutron superfluidity in the stellar core. The observed data for the neutron star in Cas A has been

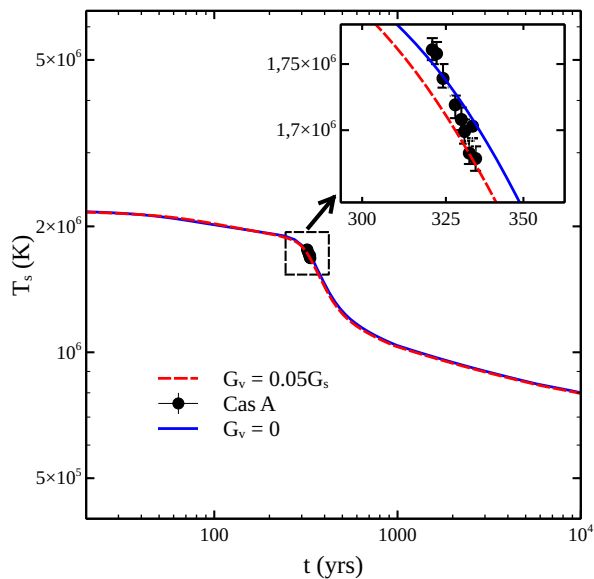


Figure 6: (Color online) Cooling curves of a  $M = 1.4 M_\odot$  neutron star computed for NL3 and vector coupling constants  $G_V = 0$  and  $G_V = 0.05 G_S$ . The inset shows the data observed for Cas A over a time period of one decade. (Data taken from [70].)

revisited recently by Ho *et al.* (2015) [70], where two new Chandra ACIS-S graded observations are presented. We note, however, that the statistical significance of Cas A observed data has been called into question, as discussed in Ref. [71].

For the models of this paper, only the  $1.4 M_\odot$  neutron star computed for the NL3 parametrization ( $G_V = 0$  and  $G_V = 0.05 G_S$ ) and with deep pairing for the protons agrees with the data observed for Cas A. The reason being that this model strongly suppresses the fast neutrino cooling processes, which is necessary to explain the thermal behavior of Cas A as discussed in [63, 64]. We show this result in Fig. 6. We note that agreement with the observed Cas A data is obtained for neutron stars with masses of  $1.4 M_\odot$ , before the onset of quark matter in the stellar core. This result is in agreement with estimates of the mass of Cas A [70], which indicates that the mass of this object is probably too low to contain quark matter.

We now confront the two NL3 models that are in agreement with Cas A (i.e.,  $G_V = 0$  and  $G_V = 0.05 G_S$  with deep proton pairing) with observed thermal data on compact stars. We use two sets of observed data (see [62] and references therein), one for age estimates based on the stars' spin-down properties, and the other based on the so called kinematic age. We note that the kinematic ages constitute more realistic age estimates as they are associated with kinematic properties of supernovae believed to be the progenitors of the neutron stars in question. For the few cases where both kinematic and spin-down ages have been estimated, large discrepancies have been found. This indicates that the spin-down age needs to

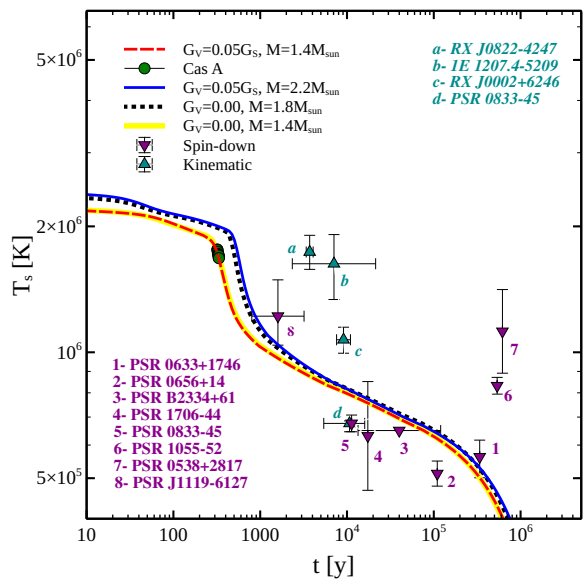


Figure 7: (Color online) Theoretical cooling curves of neutron stars, computed for NL3 and vector coupling constants  $G_V = 0$  and  $G_V = 0.05 G_S$ , compared with observed data. Pink (green) diamonds denote spin-down (kinematic) age estimates.

be considered very carefully, perhaps serving only as an upper limit on the true age of a given neutron star.

In Fig. 7, we compare the cooling tracks of neutron stars computed for the NL3 parametrization with the observed data. We note that our model agrees fairly well with some observed data, but fails to reproduce the data of several other neutron stars. This is not an inherent feature of our model but, rather, appears symptomatic for most thermal models that agree with the Cas A data (see for instance [64]). It may indicate that these objects are subjected to a heating mechanism which keeps them warm during their evolution.

## VII. SUMMARY AND CONCLUSIONS

In this work, we have used an extension of the non-local 3-flavor Nambu-Jona Lasinio model to study quark deconfinement in the cores of neutron stars. Confined hadronic matter is described by non-linear relativistic nuclear field theory, adopting two popular hadronic parametrizations labeled GM1 and NL3. The phase transition from confined hadronic matter to deconfined quark matter is modeled via the Gibbs condition, imposing global electric charge neutrality on the particle composition of neutron star matter. Repulsive forces among the quarks are described in terms of a vector coupling constant,  $G_V$ , whose value ranges from zero (no repulsion) to  $0.9 G_S$ , where  $G_S$  denotes the scalar strong coupling constant of the theory.

Each one of our models for the EoS of (quark-hybrid)



neutron star matter accommodates high-mass neutron stars with masses up to 2.4 solar masses as long as the value of  $G_V$  is sufficiently large. All high-mass stars contain extended quark-hybrid matter cores in their centers, but a pure quark matter is never reached for any of our model parametrizations. The maximum neutron star masses drop if the strength of the vector repulsion among quarks is reduced, falling below the  $2 M_\odot$  limit set by pulsars J1614 – 2230 ( $1.97 \pm 0.04 M_\odot$ ) [16] and J0348 + 0432 ( $2.01 \pm 0.04 M_\odot$ ) [17] for some parameter combinations. Examples of this are neutron stars computed for the GM1 parametrization with  $G_V = 0$ , which yields a maximum-mass neutron star of  $\sim 1.8 M_\odot$ , in conflict with the recent mass determinations mentioned just above.

The quark-hybrid stars of our study possess relatively high proton fractions in their cores so that fast neutrino processes, most notably the direct Urca process, is active, leading to very rapid stellar cooling. An agreement with the thermal evolution data of the neutron star in Cas A can be obtained, however, if one assumes that strong proton-pairing is occurring in the core of this neutron star, which is known to strongly suppress fast cooling. Under this condition, a  $1.4 M_\odot$  neutron star computed for the NL3 model and values of the vector coupling constants between  $G_V = 0$  and  $G_V = 0.05 G_S$  lead to excellent agreement with the observed data. It is important to note that the proton pairing model has not been fine tuned to the Cas A data. Further studies where we also

take into account pairing among the quarks will be presented in a future work. We have also compared the thermal behavior predicted for Cas A with that of other compact stars. In contrast to Cas A, however, these observations only temperature “snapshots” exist for the latter, with age estimates based on either their kinematic or spin-down properties. The results show that the NJL models that are in agreement with Cas A (i.e.,  $G_V = 0$  and  $G_V = 0.05 G_S$  with deep proton pairing) lead to good agreement with the observed data of several other compact objects, while failing to reproduce several other data. This, however, is not an inherent feature of our model but, rather, appears symptomatic for most thermal models that agree with the Cas A data [64].

### Acknowledgments

S.M.C. acknowledge the support by the International Cooperation Program CAPES-ICRANet financed by CAPES – Brazilian Federal Agency for Support and Evaluation of Graduate Education within the Ministry of Education of Brazil. R. N. acknowledges financial support by CAPES and CNPq. M.O. and G.C. acknowledge financial support by CONICET, Argentina. F.W. is supported by the National Science Foundation (USA) under Grant PHY-1411708.

- 
- [1] *Strongly Interacting Matter - The CBM Physics Book*, B. Friman, C. Höhne, J. Knoll, S. Leupold, R. Randrup, J. Rapp, P. Senger, (Eds.), Lecture Notes in Physics **814**, 960 pages, (Springer, 2011).
  - [2] See NICA White Paper at <http://nica.jinr.ru/files/WhitePaper.pdf>.
  - [3] N. K. Glendenning, *Compact Stars, Nuclear Physics, Particle Physics, and General Relativity*, 2nd ed. (Springer-Verlag, New York, 2000).
  - [4] F. Weber, *Pulsars as Astrophysical Laboratories for Nuclear and Particle Physics*, High Energy Physics, Cosmology and Gravitation Series (IOP Publishing, Bristol, Great Britain, 1999).
  - [5] *Physics of Neutron Star Interiors*, ed. by D. Blaschke, N. K. Glendenning, and A. Sedrakian, Lecture Notes in Physics **578** (Spring-Verlag, Berlin, 2001).
  - [6] J. M. Lattimer and M. Prakash, *Astrophys. J.* **550**, 426 (2001).
  - [7] F. Weber, *Prog. Part. Nucl. Phys.* **54**, 193 (2005).
  - [8] D. Page and S. Reddy, *Ann. Rev. Nucl. Part. Sci.* **56**, 327 (2006).
  - [9] P. Haensel, A. Y. Potekhin, and D. G. Yakovlev, *Neutron Stars 1*, Astrophysics and Space Science Library, (Springer-Verlag, New York, 2006).
  - [10] T. Klähn *et al.*, *Phys. Rev. C* **74**, 035802 (2006).
  - [11] A. Sedrakian, *Prog. Part. Nucl. Phys.* **58**, 168 (2007).
  - [12] T. Klähn *et al.*, *Phys. Lett. B* **654**, 170 (2007).
  - [13] M. G. Alford, A. Schmitt, K. Rajagopal, and T. Schäfer, *Rev. Mod. Phys.* **80**, 1455 (2008).
  - [14] F. Weber, G. A. Contrera, M. G. Orsaria, W. Spinella, and O. Zubairi, *Mod. Phys. Lett. A* **29**, 1430022 (2014).
  - [15] H. Grigorian, D. Blaschke, and D. N. Voskresensky, *arXiv:1502.03080 [astro-ph.HE]*.
  - [16] P. B. Demorest, T. Pennucci, S. M. Ransom, M. S. E. Roberts, and J. W. T. Hessels, *Nature* **467**, 1081 (2010).
  - [17] Lynch *et al.* *Astrophys. J.* **763**, 81 (2013); J. Antoniadis *et al.*, *Science* **340**, no. 6131 (2013).
  - [18] M. Orsaria, H. Rodrigues, F. Weber, and G. A. Contrera, *Phys. Rev. D* **87**, 023001 (2013).
  - [19] M. Orsaria, H. Rodrigues, F. Weber, and G. A. Contrera, *Phys. Rev. C* **89**, 015806 (2014).
  - [20] H. Chen, G. F. Burgio, H.-J. Schulze, and N. Yasutake, *Astron. Astrophys.* **551**, A13 (2013).
  - [21] H. Chen, J.-B. Wei, M. Baldo, G. F. Burgio, and H.-J. Schulze, *Phys. Rev. D* **91**, no. 10, 105002 (2015).
  - [22] D. E. Alvarez-Castillo and D. Blaschke, *arXiv:1412.8463 [astro-ph.HE]*.
  - [23] R. Lastowiecki, D. Blaschke, T. Fischer, and T. Klähn, *arXiv:1503.04832 [nucl-th]*.
  - [24] V. Dexheimer, R. Negreiros, and S. Schramm, *Phys. Rev. C* **91**, no. 5, 055808 (2015).
  - [25] F. Özel , D. Psaltis , T. Güver, G. Baym , C. Heinke, and S. Guillot, *arXiv:1505.05155*.
  - [26] S. Guillot and R. E. Rutledge, *Astrophys. J. Lett.* **796**, L3 (2014).

- [27] A. W. Steiner, J. M. Lattimer, and E. F. Brown, *Astrophys. J. Lett.* **765**, L5 (2013).
- [28] V. Suleimanov, J. Poutanen, M. Revnivtsev, and Klaus Werner, *Astrophys. J.* **742**, 122 (2011).
- [29] J. Trümper, *Prog. Part. Nucl. Phys.* **66**, 674 (2011).
- [30] J. Ellis, J. I. Kapusta, and K. A. Olive, *Nucl. Phys.* **B348**, 345 (1991).
- [31] N. K. Glendenning, *Phys. Rev. D* **46**, 1274 (1992).
- [32] G. Baym, C. J. Pethick, and P. Sutherland, *Astrophys. J.* **170**, 299 (1971).
- [33] G. Baym, H. A. Bethe, and C. J. Pethick, *Nucl. Phys. A* **175**, 225 (1971).
- [34] K. Iida and K. Sato, *Phys. Rev. C* **58**, 2538 (2008).
- [35] L. F. Palhares and E. S. Fraga, *Phys. Rev. D* **82**, 125018 (2010).
- [36] T. Endo, *Phys. Rev. C* **83**, 068801 (2011).
- [37] M. B. Pinto, V. Koch, and J. Randrup, *Phys. Rev. C* **86**, 025203 (2012).
- [38] G. Lugones, A. G. Grunfeld, and M. A. Ajmi, *Phys. Rev. C* **88**, 045803 (2013).
- [39] W. Y. Ke and Y. X. Liu, *Phys. Rev. C* **89**, 074041 (2015).
- [40] M. Alford, K. Rajagopal, S. Reddy, and F. Wilczek, *Phys. Rev. D* **64**, 074017 (2001).
- [41] N. K. Glendenning, *Phys. Rep.* **342**, 393 (2001).
- [42] S. Reddy, G. Bertsch, and M. Prakash, *Phys. Lett. B* **475**, 1 (2000).
- [43] X. Na, R. Xu, F. Weber, and R. Negreiros, *Phys. Rev. D* **86**, 123016 (2012).
- [44] Y. Nambu and G. Jona-Lasinio, *Phys. Rev.* **122**, 345 (1961); *Phys. Rev.* **124**, 246 (1961).
- [45] A. Scarpettini, D. Gomez Dumm, and N. N. Scoccola, *Phys. Rev. D* **69**, 114018 (2004).
- [46] G. A. Contrera, D. Gomez Dumm, and N. N. Scoccola, *Phys. Lett. B* **661**, 113 (2008).
- [47] G. A. Contrera, D. Gomez Dumm, and N. N. Scoccola, *Phys. Rev. D* **81**, 054005 (2010).
- [48] J. D. Walecka, *Ann. Phys.* **83**, 497 (1974).
- [49] J. Boguta and A.R. Bodmer, *Nucl. Phys.* **A292**, 413 (1977).
- [50] J. Boguta and J. Rafelski, *Phys. Lett.* **71B**, 22 (1977).
- [51] J. Boguta and H. Stöcker, *Phys. Lett.* **120B**, 289 (1983).
- [52] B. D. Serot and J. D. Walecka, *Adv. Nucl. Phys.* **16**, 1 (1986).
- [53] N. K. Glendenning and S. A. Moszkowski, *Phys. Rev. Lett.* **67**, 2414 (1991).
- [54] G. A. Lalazissis, J. König, and P. Ring, *Phys. Rev. C* **55**, 540 (1997).
- [55] D. B. Blaschke, D. Gomez Dumm, A. G. Grunfeld, T. Klahn, and N. N. Scoccola, *Phys. Rev. C* **75**, 065804 (2007).
- [56] K. Kashiwa, T. Hell, and W. Weise, *Phys. Rev. D* **84**, 056010 (2011).
- [57] G. A. Contrera, A. G. Grunfeld, and D. B. Blaschke, *Phys. Part. Nucl. Lett.* **11**, 4, 342 (2014).
- [58] A. Drago, A. Lavagno, G. Pagliara, and D. Pigato, *Phys. Rev. D* **90**, 065809 (2014).
- [59] M. Rotondo, Jorge A. Rueda, R. Ruffini, and S.-S. Xue, *Phys. Lett. B* **701**, 667 (2011).
- [60] D. Page, J. M. Lattimer, M. Prakash, and A. W. Steiner, *Astrophys. J. Suppl.* **155**, 623 (2004).
- [61] D. Yakovlev and C. Pethick, *Annu. Rev. Astron. Astrophys.* **42**, 169 (2004).
- [62] D. Page, J. M. Lattimer, M. Prakash, and A. W. Steiner, *Astrophys. J.* **707**, 1131 (2009).
- [63] D. Page, M. Prakash, J. M. Lattimer, and A. W. Steiner, *Phys. Rev. Lett.* **106**, 081101 (2011).
- [64] P. S. Shternin, D. G. Yakovlev, C. O. Heinke, W. C. G. Ho, and D. J. Patnaude, *Monthly Notices of the Royal Astronomical Society: Letters* **412**, L108-L112 (2011).
- [65] D. Blaschke, H. Grigorian, D. N. Voskresensky, and F. Weber, *Phys. Rev. C* **85**, 022802(R) (2012).
- [66] J. M. C. Chen, J. W. Clark, R. D. Davé, and W. Khodel, *Nucl. Phys.* **A555**, 59 (1993).
- [67] D. G. Yakovlev, A. D. Kaminker, U. Y. Gnedin, and P. Haensel, *Phys. Reports* **354**, 1 (2001).
- [68] A. W. Steiner, *Phys. Rev. C* **74**, 045808 (2006).
- [69] C. O. Heinke and W. C. G. Ho, *Astrophys. J.* **719**, L167 (2010).
- [70] W. C. G. Ho, K. G. Elshamouty, C. O. Heinke, and A. Y. Potekhin, *Phys. Rev. C* **91**, 015806 (2015).
- [71] B. Posselt, G. G. Pavlov, V. Suleimanov and O. Kargaltsev, *Astrophys. J.* **779**, 186 (2013).